Efficient Correction of Oncogenic *KRAS* and *TP53* Mutations through CRISPR Base Editing

Shady Sayed[1,2], Olga A. Sidorova[1], Alexander Hennig[2,4], Martina Augsburg[1], Catherine P. Cortés Vesga[1], Moustafa Abohawya[5], Lukas T. Schmitt[1], Duran Sürün[1], Daniel E. Stange[2,4,5], Jovan Mircetic[1,4,5], and Frank Buchholz[1,2,4,5]

ABSTRACT

KRAS is the most frequently mutated oncogene in human cancer, and its activating mutations represent long-sought therapeutic targets. Programmable nucleases, particularly the CRISPR-Cas9 system, provide an attractive tool for genetically targeting *KRAS* mutations in cancer cells. Here, we show that cleavage of a panel of *KRAS* driver mutations suppresses growth in various human cancer cell lines, revealing their dependence on mutant *KRAS*. However, analysis of the remaining cell population after long-term Cas9 expression unmasked the occurence of oncogenic *KRAS* escape variants that were resistant to Cas9-cleavage. In contrast, the use of an adenine base editor to correct oncogenic *KRAS* mutations progressively depleted the targeted cells without the appearance of escape variants and allowed efficient and simultaneous correction of a cancer-associated *TP53* mutation. Oncogenic *KRAS* and *TP53* base editing was possible in patient-derived cancer organoids, suggesting that base editor approaches to correct oncogenic mutations could be developed for functional interrogation of vulnerabilities in a personalized manner for future precision oncology applications.

Significance: Repairing *KRAS* mutations with base editors can be used for providing a better understanding of *RAS* biology and may lay the foundation for improved treatments for *KRAS*-mutant cancers.

Introduction

The *RAS* gene family member *KRAS* is the most frequently mutated oncogene in human cancer, with approximately 14% of patients harboring *KRAS* mutations, equivalent to approximately 2.5 million new cases per year worldwide (1, 2). Activating mutations in *KRAS* lead to a constitutively active *RAS/RAF* signaling pathway capable of inducing cell transformation by forcing cells into continuous proliferation, making the mutation an important therapeutic target (3). However, despite more than three decades of intense research efforts, targeting KRAS has proven challenging owing to its small size (~21 kDa, 189 amino acids) and a "smooth" surface that impedes binding by small molecules (2). Moreover, KRAS exhibits exceptionally high affinity to its endogenous target, GTP, leading to an extremely strong binding that prevents direct targeting of the nucleotide-binding pocket (4). Furthermore, the high intracellular GTP concentrations (>500 μmol/L) hinders competition (5). Therefore, targeting strategies have shifted away from a pan-KRAS inhibitor to an approach supporting mutation-selective approaches. Renewed hope has been brought about by the recent development of $KRAS^{G12C}$-specific inhibitors (6), which has resulted in the approval of the first $KRAS^{G12C}$-inhibitor for clinical use (7). However, other *KRAS* mutations, which are more common, such as $KRAS^{G12D}$ or $KRAS^{G13D}$ remain "undruggable" to date.

Functional genomic studies examining the expression of gene products in cancer cell lines have revealed that *KRAS*-mutant cancer cells depend on *KRAS* function for growth and survival (8). Moreover, siRNAs that selectively inhibit mutant *KRAS* mRNAs (9) led to impeded growth of cancer cells both *in vitro* and *in vivo* (10). However, continuous expression/delivery of the silencing trigger is required to maintain target RNA suppression, making this approach difficult to apply in a clinical setting. Programmable nucleases have recently been developed to selectively cleave oncogenic mutations in cancer cells. They offer the advantage of working at the genomic level and achieving permanent gene disruption (11). However, detailed long-term studies following cleavage of oncogenic mutations have not yet been reported. Furthermore, this approach is not applicable to mutations occurring in tumor suppressor genes. The recently developed CRISPR adenine base editing system is independent of DNA double-strand break repair and has recently been applied to repair a cancer-associated mutation in the *TERT* promoter (12). However, to our knowledge, it has not been tested for the correction of an activated oncogene or a mutated tumor suppressor gene to date. To examine efficiency, specificity, and durability of these approaches, we harnessed CRISPR-Cas9 systems to selectively cleave or correct different oncogenic *KRAS* variants and *TP53* hotspot mutations in a panel of cancer cell lines and patient-derived organoids (PDO) and analyzed the cells in culture over an extended period of time.

[1]Medical Systems Biology, Medical Faculty and University Hospital Carl Gustav Carus, Technische Universität Dresden, Dresden, Germany. [2]National Center for Tumor Diseases (NCT), Dresden, Germany; Faculty of Medicine and University Hospital Carl Gustav Carus, Technische Universität Dresden, Dresden, Germany; Helmholtz-Zentrum Dresden - Rossendorf (HZDR), Dresden, Germany. [3]Department of Visceral, Thoracic and Vascular Surgery, Medical Faculty and University Hospital Carl Gustav Carus, Technische Universität Dresden, Dresden, Germany. [4]Mildred Scheel Early Career Center (MSNZ) P2, National Center for Tumor Diseases Dresden (NCT/UCC), Medical Faculty and University Hospital Carl Gustav Carus, Technische Universität Dresden, Dresden, Germany. [5]German Cancer Research Center (DKFZ), Heidelberg and German Cancer Consortium (DKTK) Partner Site, Dresden, Germany.

Corresponding Author: Frank Buchholz, Medical Systems Biology, Medical Faculty and University Hospital Carl Gustav Carus, Technische Universität Dresden, Dresden, Germany. E-mail: frank.buchholz@tu-dresden.de

Cancer Res 2022;82:3002–15

doi: 10.1158/0008-5472.CAN-21-2519

Materials and Methods

sgRNA design

Since we implement a mutation-selective approach targeting point mutations, sgRNAs were manually modified to match the mutant sequence in question and manually assessed (e.g., using IDT CRISPR-Cas9 guide RNA design checker https://eu.idtdna.com/site/order/designtool/index/CRISPR_SEQUENCE). The designed sgRNAs differ in only one nucleotide from the wild-type allele sequence, making the wild-type allele the most likely off-target site. Therefore, for each experiment, mutation-selective sgRNAs were delivered to cells that do not carry the mutation to control for potential off-target toxicities.

Plasmids

For expression of Cas9 and sgRNAs from lentiviral vectors, we optimized the sequence of pL-CRISPR.EFS.GFP (a gift from Benjamin Ebert Addgene plasmid #57818; http://n2t.net/addgene:57818; RRID: Addgene_57818; ref. 13), where the tracer sequence was modified to increase sgRNA stability and enhance its assembly with Cas9 protein (14). *Streptococcus pyogenes* Cas9 and GFP were linked via P2A and were expressed from the EFS promoter, whereas the sgRNAs were expressed from the human *U6 pol III* promoter. Protospacers targeting mutations were cloned into pL-CRISPR.EFS.GFP by cloning complementary oligonucleotides into the vector. Unless a guanine was the first base in the protospacer, a guanine was added to the 5′ end of the protospacer before cloning to boost the expression of the gRNA from the human U6 promoter (15). Likewise, for ABE8e timecourses, protospacers were cloned into the LRT2B vector expressing TdTomato (a gift from Lukas Dow Addgene plasmid #110854; http://n2t.net/addgene:110854; RRID:Addgene_110854; ref. 16), using BsmBI/BbsI sites following the standard protocol (Supplementary Table S1; ref. 15). Briefly, oligos for gRNA were phosphorylated and annealed in a 10 μL reaction containing 100 pmol of each gRNA oligo (top and bottom oligos), 1 μL 10× T4 ligation buffer and 0.5 μL T4 polynucleotide kinase. The reaction was run in thermocycler at 37°C for 30 minutes, 95°C for 5 minutes, and then ramped down to 25°C at rate of 0.1°C/min. The reaction was then diluted 250 times in water and 2 μL was used for the restriction/ligation golden gate protocol. In this reaction, 50 ng backbone plasmid was added to the diluted annealed oligos together with 1 μL Tango buffer (Thermo Fisher Scientific), 0.5 μL 10 mmol/L DTT, 1 μL 10 mmol/L ATP, 0.5 μL BsmBI/BbsI, and 0.25 μL T4 DNA ligase in 10 μL final reaction. To digest the vector and ligate oligos into it, the following temperature profile was repeated six times in a thermocycler: 37°C for 5 minutes, 23°C for 5 minutes followed by incubation at 37°C for 15 minutes, and finally at 80°C for 5 minutes. Next, 2 μL of this final reaction was used to transform *DH5α Escherichia coli* cells. A single colony was picked, grown in liquid LB-antibiotic media before plasmid DNA was purified (Thermo Fisher GeneJet DNA Miniprep Kit). Plasmids were sequenced with a forward primer to the U6 promoter: 5′-GAGGGCCTATTTCCCATGATTCC-3′. For the base editor cloning, we used the plasmid backbone pLenti-FNLS-P2A-GFP-PGK-Puro (a gift from Lukas Dow Addgene plasmid #110869; http://n2t.net/addgene:110869; RRID:Addgene_110869; ref. 16), which is a lentiviral vector bearing a codon optimized CBE (BE3) in combination with GFP and the puromycin resistance gene. The CBE in the backbone was replaced with NG-ABE8e (a gift from David Liu; Addgene plasmid #138491; http://n2t.net/addgene:138491; RRID: Addgene_138491) through intermediary Acc65I and BstZ17I restriction sites. The ligation product was transformed into bacteria for overnight incubation. Single clones were picked, grown, and miniprepped followed by sequencing employing several primers aligning the full sequence of the base editor in addition to diagnostic test digests confirming the correct integration into the backbone. Finally, Plasmid DNA were transformed into *E. coli* DH5α and cells were grown overnight at 37°C with constant shaking. Plasmid DNA was purified using QIAGEN-tip 20 Maxiprep Kit (Qiagen 10023), according to the manufacturer's protocol. The DNA was resuspended at 1 μg/μL, validated by Sanger sequencing and then used for lentivirus production.

Cell culture

PANC-1 (CRL-1469), RKO (CRL-2577), HCT116 (CCL-247), A549 (CCL-185), and HEK293T (CRL-11268) cells were purchased from ATCC and maintained in DMEM (high glucose, GlutaMAX, pyruvate; Gibco) supplemented with 10% (v/v) FBS (Gibco) and antibiotics (100 U/mL penicillin, 100 μg/mL streptomycin; Gibco) and kept at 37°C, 5% CO_2. Cell lines were routinely tested and confirmed to be *Mycoplasma*-free (latest on June 1, 2022). For all cell lines used, cells were allowed to recover after thawing for two passages before performing experiments.

TA cloning

TA cloning was performed using the TA Cloning Kit with pCR2.1 vector (Thermo Fisher Scientific). The amplicons were separated using agarose gel electrophoresis and the target bands were extracted and purified using the Gel extraction Purification Kit (Bioline). The DNA concentration was measured with a Nanodrop spectrophotometer. For TA cloning ligation, 0.1 to 0.3 pmol of DNA fragments were mixed with pCR2.1 vector according to manufacturer's protocol, incubated at 16°C for 1 hour. The ligation product was transformed into competent *E. coli* DH5α employing blue/white screening. White colonies were picked the next day and plasmid DNA was extracted via Mini-prep. Finally, PCR reactions using M13 forward and reverse primers were performed, followed by Sanger sequencing.

Lentivirus production and transduction

Lentiviral particle production and infection were performed as described previously (17). Briefly, seven million HEK293T cells were seeded in 10 cm dishes and transfected on the next day at ∼80% confluency with 2 μg pMD2.G (a gift from Didier Trono Addgene plasmid #12259; http://n2t.net/addgene:12259; RRID:Addgene_12259), 6 μg psPAX2 (a gift from Didier Trono Addgene plasmid #12260; http://n2t.net/addgene:12260; RRID:Addgene_12260) and 10 μg of the transfer vector (e.g., pL-CRISPR.EFS.GFP.gRNA) using 45 μg PEI (1 mg/mL) per dish. Plasmid maxiprep kits (Qiagen) were used to provide transfection-level DNA. After ∼20 hours of transfection, the medium was changed to complete DMEM and 72 hours after transfection the viral supernatant was collected, filtered through a 0.45 μmol/L filter and centrifuged for 2 hours at 100,000 × *g* at 4°C. The supernatant was decanted and the viral pellets were resuspended in PBS overnight at 4°C on a shaker. For long-term storage, the virus particles were kept in cryovials at −80°C. Where indicated, the viral supernatant was concentrated using Amicon Ultra-15 Centrifugal Filter Devices (Merck) according to the manufacturer's instructions. When a new cell line was used for the first time, the amount of virus needed to infect 50% of the cells was determined by titration. Transductions were typically performed in 96-well plates in the presence of protamine sulfate (final concentration 5 μg/mL; Sigma-Aldrich) and spin-infected for 1 hour at 1,000 × *g* at 37°C.

Flow cytometry

RKO, PANC-1, A549, and HCT116 were typically transduced in 96-well plates and the percentage of infected cells was analyzed measuring GFP/TdTomato expression using a MACSQuant VYB Analyzer (Miltenyi Biotec). At 72 hours after transduction, cells were trypsinized and collected for flow cytometry analysis. Viable single cells were gated using the forward and side scatter followed by doublets exclusion. The BFP fluorescence signal was measured using a violet 405 nm laser, the GFP fluorescence signal was measured using a blue 488 nm laser, whereas the TdTomato was assayed using a 561 nm yellow laser and the log area of the signal was collected. Cell sorting was carried out using a BD FACSAria III Cell Sorter (BD Biosciences). For time course experiments, adherent cells were processed every 48 to 72 hours by flow cytometry in technical triplicates. Briefly, for each time point, medium was aspirated completely using a multichannel pipette. Then, cells were carefully washed with 200 μL sterile PBS and treated with 30 μL/well trypsin, enough to cover the adherent layer of cells. Cells were incubated for 5 minutes at 37°C. Next, 170 μL complete medium was added directly to the cells. The cell suspension was homogenized by pipetting up and down vigorously. Then, 30 μL was transferred to a new 96-well plate for later acquisitions, filled up to 200 μL with prewarmed complete medium. Of the remaining 170 μL cell solution, 50 μL was used for flow cytometry acquisition and the rest was used for gDNA isolation.

Human organoids culture

Human PDOs were derived from resection material of pancreatic ductal adenocarcinoma (PDAC), colorectal carcinoma, and patients with gastric cancer who underwent surgery at the Department of Visceral, Thoracic and Vascular Surgery at the University Hospital Carl Gustav Carus of the TU Dresden. The study was approved by the Ethical Committee of the TU Dresden (#EK451122014). PDAC, colorectal cancer, and gastric cancer PDOs were cultured as described earlier (18, 19) and mutations were verified by Sanger sequencing. For passaging, PDOs from three to four wells from a 48-well plate were pooled in a 15 mL reaction tube and mechanically dissociated by repeated pipetting up and down through a fire-polished glass pipette. After centrifuging 5 minutes at 300 × *g*, the supernatant was aspirated and the pellet resuspended in Matrigel before plating as 20 μL drops in a new 48-well plate. Subsequently, Matrigel drop polymerization was induced by incubating for 10 minutes at 37°C and 250 μL organoid medium added to each well. For long-term storage, organoids were disrupted as for passaging using the Pasteur pipette. Fragments were dispensed in cold Recovery Cell Culture Freezing Medium (500 μL/well) and placed in 1 mL cryotubes. PDOs were frozen overnight in −80°C freezer in a cryo-freezing container (Mr. Frosty, Nalgene). On the next day, cells were transferred to liquid nitrogen. For thawing, cryotubes were warmed at 37°C and cells were resuspended in 10 mL advanced DMEM/F12 and then centrifuged for 5 minutes at 300 × *g*. Pelleted cells were resuspended in 20 μL Matrigel and placed in a well of a pre-warmed 48 well plate and placed at 37°C for 10 minutes. Finally, the Matrigel drop was overlaid with 250 μL of prewarmed medium containing all growth factors including RHOKi.

Genotyping of base edited cells

Genomic DNA was isolated using the QIAamp DNA Blood Mini Kit according to manufacturer's instructions. Targeted *KRAS* exon2 or *TP53* exon7 PCR amplification was performed using high-fidelity Phusion polymerase using the following protocol:

Nuclease-free water up to 50 μL
10 μL HF buffer
1 μL dNTP mix (10 mmol/L each)
1,25 μL 20 μmol/L (FwdPrimer)
1,25 μL 20 μmol/L (RevPrimer)
250ng gDNA or 0.5 μL cell lysate
0.5 μL Phusion DNA polymerase

Reagents were mixed, briefly spun down at room temperature and run in a thermocycler with the following cycling conditions:

1 cycle: 30 seconds 98°C (initial denaturation)
30 cycles: 10 seconds 98°C (denaturation)
20 seconds 65°C (annealing, specific to primer pairs)
30 seconds 72°C (extension)
1 cycle: 5 minutes 72°C (final extension)
1 cycle: ∞ 8°C (hold).

A 5-μL aliquot of each PCR reaction was run on agarose gel, confirming correctly-sized bands and purity of procedure through a blank no-template water control. PCR products were purified using ISOLATE II PCR and Gel Kit (Bioline) according to manufacturer's instructions and DNA concentrations were quantified using a Nanodrop spectrophotometer. The appropriate amount of DNA together with the respective sequencing primers (forward or reverse primer were used) were submitted for Sanger sequencing, following the vendor's protocol.

EditR to quantify base editing efficiency

EditR is a free online tool (20) to quantify sequencing reads from raw ab1 files. For quantification of *KRAS* base editing, we amplified a 544 bp PCR product spanning *KRAS* residues 12 and 13 of the gRNA-treated cells. Cells transduced with the nontargeting gRNA were used as control. The obtained ab1 files of the potentially edited region was uploaded to EditR together with the gRNA protospacer sequence (∼20 bp). EditR generated plots displaying editing efficiencies at each base within the protospacer.

Cell-cycle analysis

PANC-1 cells expressing ABE8e-GFP were seeded in a 24-well plate and transduced with the gRNA-tdTomato construct as described above. The cell-cycle assay was performed 7 days after infection with the Click-iT EdU Alexa Fluor 647 Flow Cytometry Assay Kit (Invitrogen; Thermo Fisher Scientific), according to the manufacturer's instructions. To stain for the total DNA content, fxCycle Violet stain (Invitrogen; Thermo Fisher Scientific) was used at a 1:1,000 dilution. The flow cytometry was carried out on a MACSQuant X (Miltenyi Biotec), followed by the analysis of the acquired data with the FlowJo software (FlowJo, RRID:SCR_008520).

Time-lapse microscopy

PANC-1-ABE8e-GFP sorted cells expressing the base editor were infected with pLenti.sgG12D-1-TdTomato, at MOI = 1, resulting in ∼50% infection rate to create an internal competition between cells bearing the base editing gRNA and cells expressing only the base editor. Four days after infection, cells were seeded into a μ-Slide 8 well-chambered coverslip slide (Ibidi) containing 300 μL of FluoroBrite DMEM (Gibco) supplemented with 10% FBS, 4 mmol/L GlutaMAX, and 1% Pen/Strep. Time-lapse microscopy-based imaging was performed over 5 days using the Deltavision Elite deconvolution microscope. Images were acquired on FITC, TRITC, and Cy5 channels every 30 minutes using a 20×/1.42 plan-Apochromat objective, at 37°C with

5% CO_2. Subsequently, images were deconvolved and z-projected using softWoRx analysis software (SoftWoRx, RRID:SCR_019157).

Statistical analysis

Data were analyzed using GraphPad Prism version 6 (GraphPad Prism, RRID:SCR_002798). Unless otherwise stated, time points in time-course experiments are presented as the SDs (presented as error bars) of three independent experiments, performed in biological triplicates. For base editing timecourses, the raw FACS points were processed using functions implemented in RStudio Version 1.2.1335 (RStudio, RRID:SCR_000432) and the statistical difference between the mean percentage at end-point of experimental gRNA and that of nontargeting gRNA/no gRNA was determined using unpaired two-tailed Student t test. A $P < 0.05$ was considered to be statistically significant.

Deep sequencing of potential off-target editing

Pooled sequencing reads were demultiplexed using the cutadapt software package. Fastq files generated were analyzed using CRISPResso2 (21) to calculate editing frequencies on both ON and OFF target sites. To calculate A to G editing efficiencies, we added the frequencies of all alleles that has at least one A converted to G in the quantification window, which is defined as −10 and +10 from the center of the gRNA. For quantification of DNA edits via nanopore sequencing, PCR products from target regions were sequenced with the native barcoding approach using SQK-LSK109 and EXP-NBD104 on a r9.4.1 flowcell (Oxford Nanopore Technologies). Sample preparation was done according to manufacturer's protocol (Version: NBA_9093_v109_revD_12Nov2019) and sequencing was performed for 24 hours. Basecalling and demultiplexing was performed with guppy v5.0.7 (Oxford Nanopore Technologies) using the dna_r9.4.1_450bps_sup model. The reads were filtered via filtlong v0.2.0 (https://github.com/rrwick/Filtlong) for a minimum mean phred score of 17 and minimum length 400 bp. DNA sequences were then mapped on the reference sequence from the PCR fragment (chr12:25,245,072–25,245,615, GRCh38/hg38) with minimap2 (version 2.17-r974-dirty; ref. 22). The edited region around Glycine 12 and Glycine 13 was then extracted from the alignments in R (version 4.1.2) via the stackStringsFromBam function from the R-package GenomicAlignments (version 1.30.0; ref. 23). The extracts were then converted to amino acid sequence with the bioseq package (version 0.1.3) and further counted and visualized using tidyverse packages (version 1.3.1).

RNA-seq analysis

Paired-end RNA-seq data were mapped to human genome hg38 from genecode https://www.gencodegenes.org/human/ with STAR_2.6.1d aligner (STAR, RRID:SCR_004463; ref. 24). First, STAR was used to build a genome index from the human genome fasta file. We then mapped reads of each sample in paired end mode. We analyzed two biological replicates for each of the three samples (RKO, RKO-ABE8e, and RKO-ABE8e-sgG12D-1). The output bam files were later indexed with the samtools software package (SAMTOOLS, RRID:SCR_002105).

To calculate the percentage of A-to-I editing in each sample, we used REDItools v1.3 (REDItools, RRID:SCR_012133; ref. 25) to quantify percentage of A to I out of total adenosines in each RNA-seq dataset. The REDItoolDenovo.py script was used to output the empirical distribution of all possible substitutions in each RNA-seq dataset. REDItools v1.3 was run on the bam files generated in the first step according to the following parameters; min mapping quality 30, min per base quality 25, min read coverage 10. Finally, we calculated the percentage of A to I editing by dividing the number of A to G substitutions (AG) over the total number of adenosines in the dataset (AA). These percentages were used to calculate the mean, SD and perform unpaired t test of two biological replicates in each sample using the GraphPad online calculator https://www.graphpad.com/quickcalcs/ttest1.cfm (GraphPad Prism, RRID:SCR_002798).

Data availability

The datasets generated during and/or analyzed during this study are available from the corresponding author F. Buchholz on request. Researchers interested in accessing the data can contact F. Buchholz at frank.buchholz@tu-dresden.de. It can take a few months to negotiate data use agreements and gain access to the data with Data Use Agreements with the Technical University of Dresden, Germany.

Results

CRISPR/Cas9-mediated cleavage of *KRAS* mutations promotes the appearance of oncogenic escape variants

To examine the precision and versatility of CRISPR/Cas9 nuclease to target different *KRAS* mutations in a panel of cancer cell lines, we tested some of the most prevalent *KRAS* mutations G12D (PANC-1), G13D (HCT116), and G12S (A549), employing a cellular fitness competition assay (**Fig. 1A**). In this assay, reduction of the percentage of GFP-positive cells over time indicates that the infected cells expressing the nuclease–sgRNA complex have a growth disadvantage in comparison with the noninfected cells. To correct for possible off-target cleavage of the *KRAS* wild-type (WT) locus, we included a *KRAS*-WT cell line as a negative control. Interestingly, although the employed sgRNAs did not show appreciable effects in the *KRAS*-WT control cell line (Supplementary Fig. S1A), the percentage of GFP-positive cells progressively declined over time in all three cell lines bearing the mutation-targeting sgRNA, suggesting that disruption of mutant *KRAS* impaired their further growth (**Fig. 1B–D**). Hence, CRISPR/Cas9-mediated cleavage of oncogenic mutations can be used to probe the dependence of the tumor cells on the mutation. However, although the noninfected cells outcompeted the targeted cells in the pool, we noticed that the depletion curves flattened at a low percentage of GFP-positive cells after prolonged culturing, an observation seen across all three tested cell lines. Of note, these persistent cells appeared healthy and proliferated in the culture for several weeks despite carrying the mutation-targeting sgRNA and Cas9. To investigate the *KRAS* locus of these cells, we sorted the residual HCT116 GFP-positive cells followed by sequencing of the PCR product of the *KRAS* locus (**Fig. 1E**). Interestingly, about half of all the reads matched the wild-type KRAS allele sequence. This was expected, because HCT116 cells are heterozygous for the G13D mutation with the second allele being *KRAS* wild type. The fact that about 50% of the sequence reads reflected *KRAS* wild type suggests the wild-type sequence is not cleaved employing this sgRNA, likely owing to the employed proximal SpCas9 NGG PAM. Analyzing the mutant allele, we observed that 13% of cells still carried the original G13D mutation, not offering a clear-cut explanation why these cells survived the continuous targeting. In contrast, 8% of the clones showed other well-known cancer driver mutations of *KRAS*, including G13V, G12S, and K16E (**Fig. 1E**). Deep sequencing of the amplified DNA fragment confirmed the emergence of these alternative *KRAS* cancer driver mutations and identified additional ones (e.g., G13Y; Supplementary Fig. SS1B). These mutants were probably induced as a consequence of G13D mutation targeting, likely through double-strand DNA break (DSB) formation, followed by

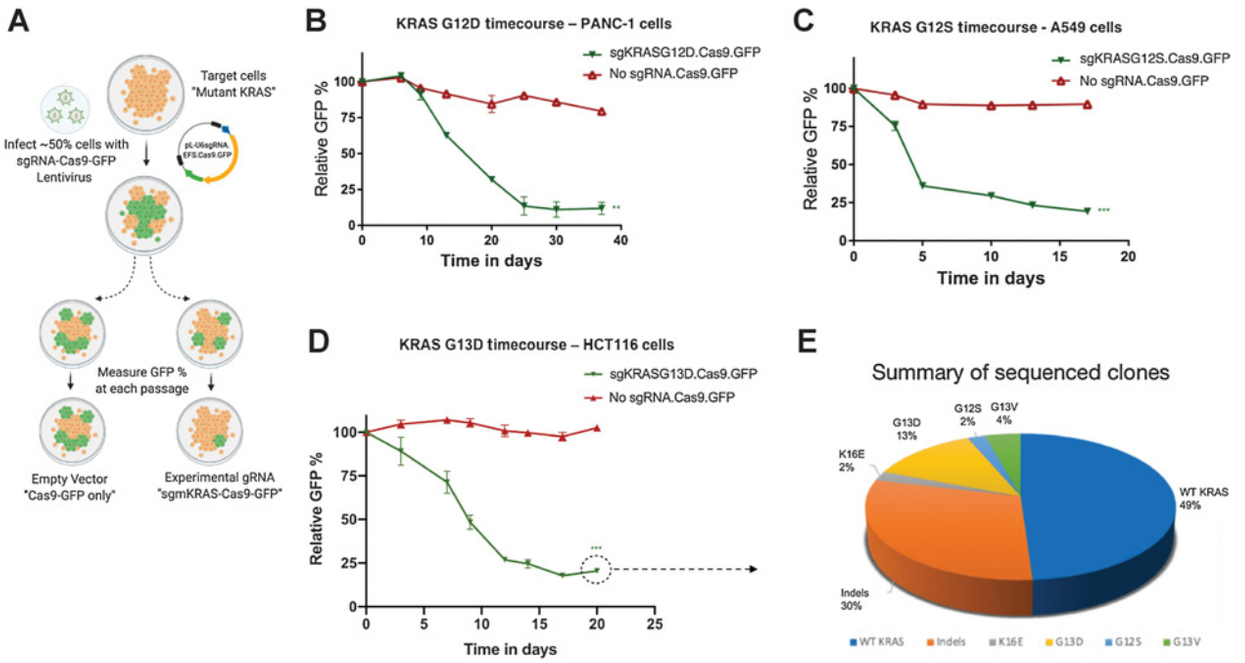

Figure 1.

CRISPR-Cas9 cleavage of different mutant *KRAS* alleles. **A,** Schematic presentation of the competition assay. Mutant cells are transduced at a rate of ~50% with an all-in-one sgRNA-Cas9-GFP lentivirus designed to target the mutation. Relative abundance of the transduced population (GFP+ cells) is measured over time via flow cytometry. **B–D,** Relative abundance of cells treated with indicated sgRNA targeting *KRAS* G12D, G12S, G13D mutation in PANC-1, A549, and HCT116 cells, respectively, is shown over time as a function of GFP% relative to day zero. In all three experiments, the day zero time point refers to 3 days after infection, the initial time point for measuring GFP signal. Note that in PANC-1 and HCT116 cell lines, the GFP signal increased slightly after the initial time point, likely because more cells started to express the fluorescent transgene, resulting in relative GFP levels above 100%. Error bars present mean ± SD from experiments performed in technical triplicates. Significance was assessed using the Student *t* test comparing the mean percentage at end point of experimental sgRNA to that of no sgRNA. **, $P < 0.005$; ***, $P < 0.0005$. The dotted circle/arrow marks the time point of analyzing GFP+ clones for their KRAS-WT allele. **E,** Genetic makeup of persisting GFP+ cells at the *KRAS* cleavage site. The pie chart represents the sum of mutations observed at the codon 13 cut site.

error-prone cell intrinsic DNA break repair in the HCT116 cells. Importantly, these mutant alleles are resistant to targeting by the initially designed sgRNA and therefore escaped the inactivation of the G13D driver mutation. We conclude that while the approach of using Cas9 nucleases to inactivate cancer mutations is efficient and informative, emerging oncogenic variants at the cleavage site will likely hamper this approach for many future applications, including potential clinical usage. Furthermore, nucleases are not useful for mutations occurring in tumor suppressor genes, because cleavage of these mutations is unlikely to reconstitute their wild-type activity.

Base editing corrects the G12S *KRAS* mutation in A549 cells

Base editing has emerged as a technology that allows precise genome editing without the introduction of DSBs (26). Relevant to this work, the described G12D, G13D, and G12S point mutations in the cell lines are potentially all addressable by an adenine base editor (ABE; Supplementary Fig. S2). We therefore decided to test whether inactivation of *KRAS* mutations using adenine base editing was feasible. Owing to the lack of a well-positioned *Sp*Cas9 NGG PAM, we decided to use a less restrictive Cas9 variant that utilizes an NG PAM (27). To enable efficient base editing, we combined this nCas9 variant with the recently described enhanced base editor ABE8e (28), hereafter referred to as NG-ABE. To allow stable expression, the *KRAS* mutant cell lines were first infected with a lentivirus expressing NG-ABE, in combination with a puromycin resistance cassette and GFP (**Fig. 2A**). The NG-ABE expressing cells were then subjected to a cell competition assay, analogous to the prior Cas9-nuclease experiments. Half of the cells were infected with a lentivirus expressing the mutant *KRAS*-specific sgRNA together with TdTomato to monitor the percentage of sgRNA-positive cells over time (**Fig. 2A**). We first tested this approach with four different sgRNAs in the human lung carcinoma cell line A549, harboring a homozygous *KRAS* G12S mutation (**Fig. 2B**). Interestingly, although the percentage of TdTomato-positive cells did not change over time in cells transduced with a no gRNA-TdTomato control, all four targeting sgRNAs led to a progressive loss, although with different kinetics, of TdTomato-positive cells over time (**Fig. 2C**), suggesting that correction of mutant *KRAS* back to the wild-type sequence impaired cell proliferation. Twelve days after infection, we isolated gDNA from the pool of cells infected with sgG12S-2-TdTomato. After PCR-amplification of *KRAS* codon 12 and Sanger sequencing, analysis revealed substantial editing at the targeted adenine ("A"), indicating conversion of the mutation back to the wild-type sequence (**Fig. 2D**; Supplementary Fig. S3). Importantly, RKO-ABE8e cells (*KRAS* WT) were not affected by infection with any of the four sgRNAs (Supplementary Fig. S4B), suggesting that targeting mutant *KRAS* with ABE8e-sgG12S did not affect proliferation of *KRAS* WT cells.

Moderate *KRAS* G13D base editing and prominent bystander edits in HCT116

Next, we tested six sgRNAs in the human colon cancer cell line HCT116, harboring a heterozygous *KRAS* G13D mutation (**Fig. 3A**).

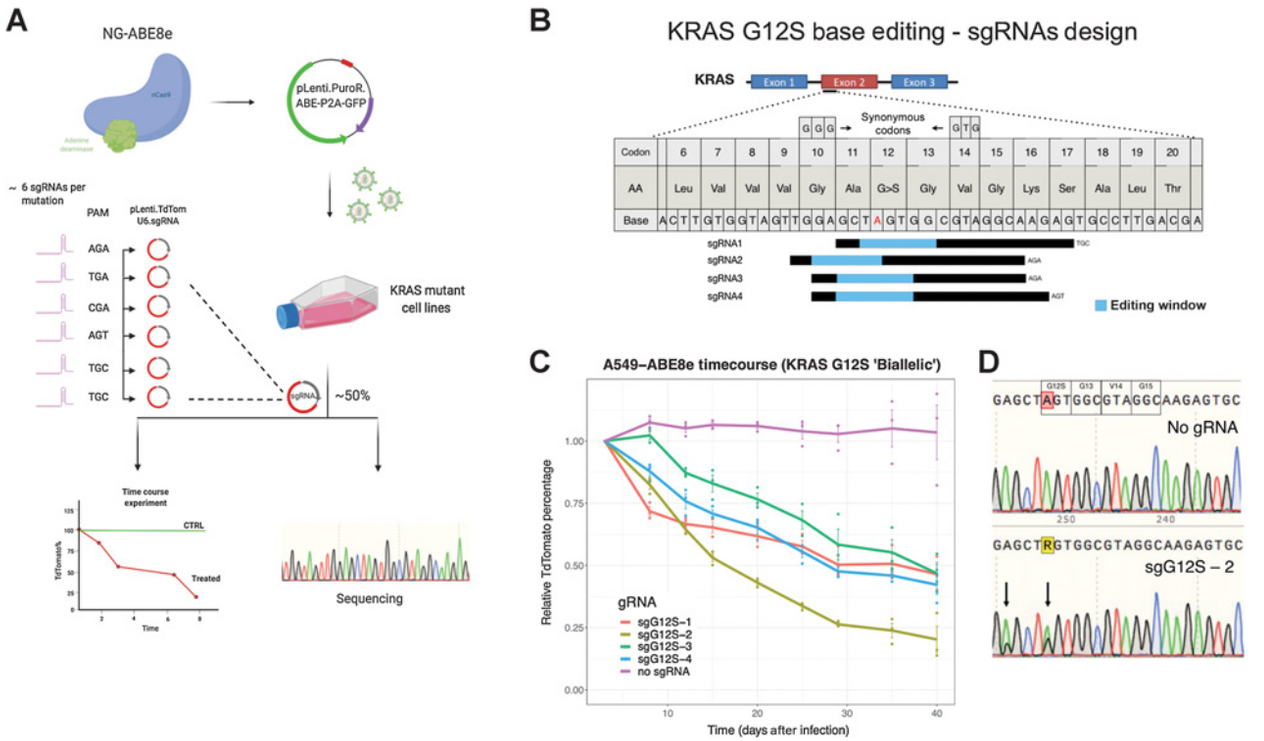

Figure 2.

Base editing of mutant *KRAS* G12S in A549 cells. **A,** Schematic presentation of the adenine base editing strategy. Important steps are highlighted by arrows. **B,** Overview of the employed sgRNAs to repair the G12S mutation. sgRNA alignments with respect to the mutation (red "A") are shown. The hypothetical editing window (blue) and the chosen PAM sequences are presented. Potential bystander base editing of surrounding A-bases (G10 and V14) would yield the same amino acid due to synonymous codons (two small arrows). AA, amino acid. **C,** Time course of *KRAS* G12S base editing in A549 cells with indicated sgRNAs. The relative abundance of cells treated with mutation-targeting gRNAs or an empty vector control are shown as percentage of TdTomato-positive cells over time, relative to 3 days after infection. Error bars represent means ± SD from biological triplicates performed in three independent experiments. **D,** Representative chromatograms of sequenced DNA isolated from cells treated with sgG12S-2 (bottom) in comparison with cells treated with empty vector control (top) 12 days after infection. The G12S homozygous mutation is highlighted in a red box. In the bottom panel, arrows highlight editing activity shown as "G" peaks in black. Note the synonymous bystander edit at a second "A."

Only one of the six tested sgRNAs (sgG13D-6) showed a continuous depletion of TdTomato-positive cells over time (**Fig. 3B**), suggesting that many sgRNAs do not function efficiently to correct the G13D mutation. Twelve days after infection, we isolated gDNA from the pool of cells infected with sgG13D-6-TdTomato, showing a depletion down to 25% at the end of the experiment. After PCR-amplification, which included *KRAS* codon 13, and Sanger sequencing, analysis revealed moderate editing at the targeted "A" (**Fig. 3C**). In addition to the targeted adenine, two adjacent "A"s were also noticeably changed as bystander edits (**Fig. 3C**). Although the altered "A" at V14 results in a silent mutation, conversion of the "A" at K16 leads to a nonsynonymous mutation, potentially creating an oncogenic *KRAS* isoform.

Efficient *KRAS* G12D base editing in PANC-1 cells

Finally, we tried to address the most frequent *KRAS* mutation—G12D and to this goal, we tested six sgRNAs in a human carcinoma cell line of the exocrine pancreas, PANC-1, harboring a heterozygous *KRAS* G12D mutation (**Fig. 4A**). In four of six sgRNAs, a rapid depletion of TdTomato-positive cells was observed, reaching depletion levels down to 1% with two different sgRNAs, suggesting that the infected cells are largely outcompeted by noninfected cells (**Fig. 4B**). PCR amplification of *KRAS* codon 12 in cells infected with sgG12D-1-TdTomato at early time points after infection and subsequent Sanger sequencing revealed a high ratio of A>G conversions, signifying efficient and rapid correction back to wild-type *KRAS* sequence (**Fig. 4C**; Supplementary Fig. S5A). Importantly, potential bystander edits of adjacent "A"s would not change the protein sequence (**Fig. 4A** and **C**). Similar to our previous findings, all the tested sgRNAs showed no growth retardation in RKO-ABE8e cells (*KRAS* WT), ruling out the possibility that the effects seen are due to off-target effects (Supplementary Fig. S4A). To investigate a potential emergence of other oncogenic *KRAS* mutations, as observed in the nuclease treated cells, we sorted the remaining TdTomato-positive cells 60 days after infection, followed by gDNA isolation and sequencing of the *KRAS* locus. Remarkably, all of the sequenced clones harbored the *KRAS* wild-type sequence (Supplementary Fig. S5B), demonstrating the high accuracy of the base editor to correct the oncogenic mutation. However, this result also suggests that some rare PANC-1 cells can survive the correction of the *KRAS* mutation and continue to proliferate in culture.

Phenotypic characterization of *KRAS* G12D correction

The depletion of sgRNA-expressing cells could be caused by different scenarios, such as slowed cell growth, cell-cycle arrest, or cell death. As oncogenic KRAS is known to regulate critical components involved in cell cycle (29, 30), we first characterized the cells with corrected *KRAS* locus by performing cell-cycle analyses. Indeed, we

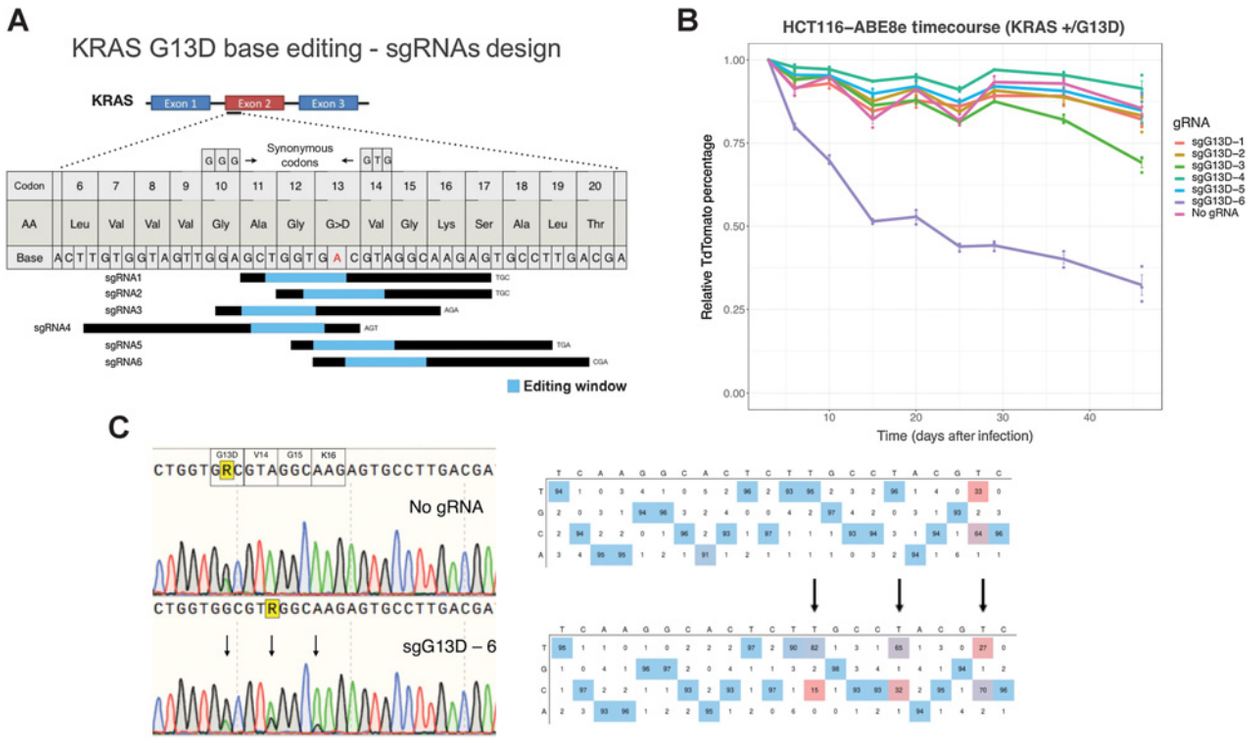

Figure 3.

Base editing of mutant *KRAS* G13D in HCT116 cells. **A,** Overview of the employed sgRNAs to repair the G13D mutation. sgRNA alignments with respect to the mutation (red "A") are shown. The hypothetical editing windows (blue) and the chosen sgRNA lengths and PAM sequences are presented. Potential bystander base editing of surrounding A-bases is illustrated as synonymous/nonsynonimous codons. **B,** Time course of *KRAS* G13D base editing in HCT116 cells with indicated sgRNAs. The relative abundance of cells treated with six sgRNAs in addition to an empty vector control is shown as percentage of TdTomato-positive cells over time, relative to 3 days after infection. Error bars represent means ± SD from biological triplicates performed in three independent experiments. **C,** Left, representative chromatograms of cells treated with sgRNA6 (bottom) in comparison with cells treated with empty vector control (top) 12 days after infection. The G13D mutation is highlighted in a yellow box. Edited "A"s, including bystander edits, are indicated by arrows in the bottom panel. Right, EditR quantification of base editing efficiency indicating the 22 bp sgG13D-6 sequence, representing base percentages of the empty vector control (top) and edited base percentages in cells treated with sgG13D-6 (bottom).

observed a decrease in proliferating cells reflected by a significant increase in the fraction of cells in G_0–G_1 phase of the cell cycle (**Fig. 4D**). In line with existing work (31), this result indicates that mutant *KRAS* is required for G_1 progression to S phase. Sequencing of infected cells at an early time point (3 days after infection) revealed that the base editing reaction is rather rapid (>50% at 3 dpi; Supplementary Fig. S5A). This rapid correction contrasted the relatively slow decline of gRNA expressing cells in the competition assay (∼80% Tomato-positive at day 3 after infection). To investigate the dynamics of corrected cells, we performed long-term time-lapse microscopy, where the GFP-sorted PANC-1 cells expressing NG-ABE were infected at a ratio of ∼50% with the sgG12D-1-TdTomato virus and cultured over 5 days. Intriguingly, we observed numerous cells carrying the base editing sgRNA-TdTomato that rounded up and bursted in the time-lapse movies (**Fig. 4E**; Supplementary Movie S1), indicating that some edited cells undergo cell death. Of note, a few other TdTomato-positive cells seemed to prolifate at a regular rate, indicating that these cells (even though many of them presumably carry already the *KRAS* wild-type sequence) were not affected, yet. Importantly, cells infected with control sgRNA-TdTomato continued to divide at a regular rate as observed in the time-lapse movies (Supplementary Movie S2). Taken together, these experiments indicate that the expression of mutant *KRAS* is required for continuous cell proliferation and that correction of mutant *KRAS* using base editing leads to G_0–G_1 cell-cycle arrest and sporadic cell death in corrected cells.

Off-target analysis of ABE8e targeting *KRAS* G12D mutation

To assess possible unintended editing at potential DNA sites with homology to the employed *KRAS* sgRNA, we identified most likely human off-targets using Cas-OFFinder (**Fig. 5A**; ref. 32). The top 9 potential off-target sites were PCR amplified from PANC-1-ABE8e expressing cells before and after infection with the top-performing sgRNA-1 for *KRAS*G12D mutation correction, followed by deep sequencing. Analysis of more than one million sequencing reads revealed greater than 50% A>G mutational correction for the on-target (Supplementary Fig. S6A), consistent with data obtained using EditR. In contrast, no appreciable changes at any of the off-target sites were detected (**Fig. 5B**), echoing previous reports that ABEs are rather specific (33).

Base editors might also cause off-target editing at mRNA level (34). To investigate possible deamination of adenines in a transcriptome-wide manner, we isolated mRNA from control cells and cells stably expressing ABE8e and the top-performing sgRNA-1 for the G12D mutation. We then measured the A-to-I substitution frequency across the transcriptome for the samples by deep sequencing. Analyzing more than 30 million reads for each sample, we did not

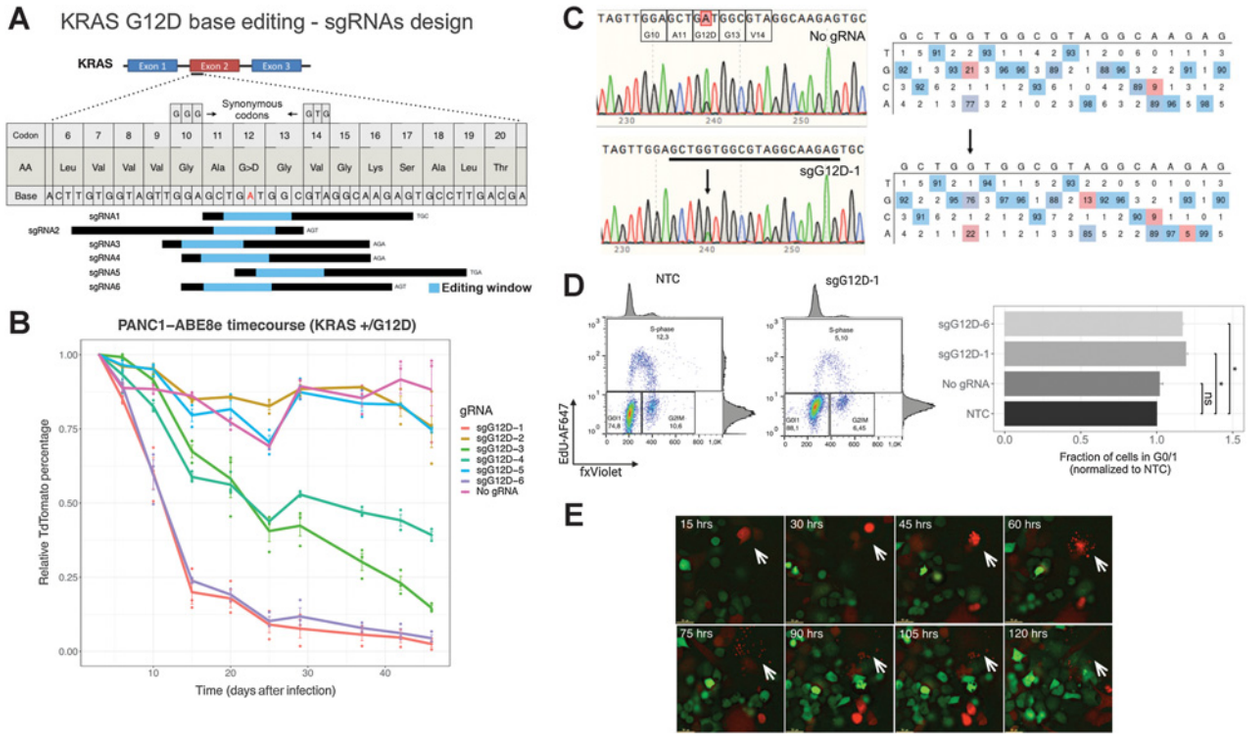

Figure 4.

Base editing of mutant *KRAS* G12D in PANC-1 cells. **A,** Overview of the employed sgRNAs to repair the G12D mutation. sgRNA alignments with respect to the mutation (red "A") are shown. The hypothetical editing windows (blue) and the chosen PAM sequences are presented. Potential bystander base editing of surrounding A-bases is illustrated as synonymous codons. **B,** Time course of *KRAS* G12D base editing in PANC-1 cells with indicated sgRNAs. The relative abundance of cells treated with six sgRNAs in addition to an empty vector control is shown as the percentage of TdTomato-positive cells over time, relative to 3 days after infection. Error bars represent means ± SD from biological triplicates performed in three independent experiments. **C,** Left, representative chromatograms of cells treated with sgRNA1 (bottom) in comparison with cells treated with the empty vector control (top) at 7 days after infection. The G12D mutation is highlighted in a red box. The edited "A" is indicated by an arrow. Right, EditR quantification of base editing efficiency indicating the 20 bp sequence of sgRNA-1, representing base percentages of the empty vector control (top) and edited base percentages in cells treated with sgRNA1 (bottom). The edited "A" is indicated by an arrow. **D,** Left, representative FACS plots showing the cell-cycle distribution of PANC-1 treated with highlighted sgRNAs. NTC, nontargeting gRNA control. Right, cell-cycle analyses of PANC-1-ABE8e cells after indicated treatments ($N = 2$). **E,** Time-lapse microscopy analysis of treated PANC-1-ABE8e cells. Representative time stamps of PANC-1 cells stably expressing ABE8e (green) after infection with sgG12D-1-TdTomato (red) are shown. White arrows, bursting cell. Scale bar, 50 μm.

detect significant differences in A-to-I conversion in transcriptomes between WT cells, cells expressing ABE8e alone, or cells expressing ABE8e together with the sgRNA (**Fig. 5C**), consistent with previous data demonstrating neglectable mRNA off-target editing of latest generation ABEs (28).

Efficient *TP53* R273H base editing in PANC-1 cells

On the basis of the success of base editing mutations in the activated oncogene *KRAS*, we thought to apply this technology to another class of genes frequently mutated in cancer cells. Tumor suppressor genes are genes that regulate cells during replication and cell division. The tumor suppressor gene *TP53* is the most frequently mutated gene in cancer (35), and like *KRAS*, it is notoriously difficult to target with conventional pharmacologic approaches (36). What is more, targeting of mutations in tumor suppressor genes with nucleases is not useful, as cleavage of the mutation is unlikely to recover the wild-type activity of the tumor suppressor gene. We therefore decided to test, whether base editing could be applied to correct mutations in *TP53* and if so, what consequences this correction might have. Of note, PANC-1 cells harbor an inactivating hotspot mutation in *TP53* (p.R273H, c.818G>A). Importantly, this mutation should be addressable by ABEs (**Fig. 6A**). As loss of tumor suppressors function often occurs through loss of heterozygosity (35), correction of only one allele might be sufficient to revert the phenotype. Towards testing this hypothesis, we cloned one sgRNA into the TdTomato lentiviral vector to repair the R273H mutation in PANC-1 cells, harboring a hemizygous *TP53* mutation. Remarkably, swift depletion of TdTomato-positive cells was observed, suggesting that the infected cells were depleted and largely outcompeted by noninfected cells (**Fig. 6B**). Moreover, PCR amplification of *TP53* exon seven 3 days after infection with sgR273H-TdTomato and subsequent sanger sequencing revealed ∼79% of A>G conversions, signifying an efficient and rapid correction back to the wild-type *TP53* sequence (**Fig. 6C**). To investigate whether *TP53* DNA correction in the genome restored its protein function, we performed RT-qPCR for a panel of p53 target genes. Interestingly, rapid induction of expression was observed for *p21*, an early, canonical transcriptional target of p53, regulating cell cycle and apoptosis (**Fig. 6D**). Furthermore, other key p53 target genes inducing cell growth arrest such as *MDM4* and DNA damage inducible gene *GADD45A*, as well as the apoptosis regulator *PUMA*, were upregulated (**Fig. 6D**), indicating that restoration of wild-type p53 reactivates its function as a gatekeeper for cell growth and division.

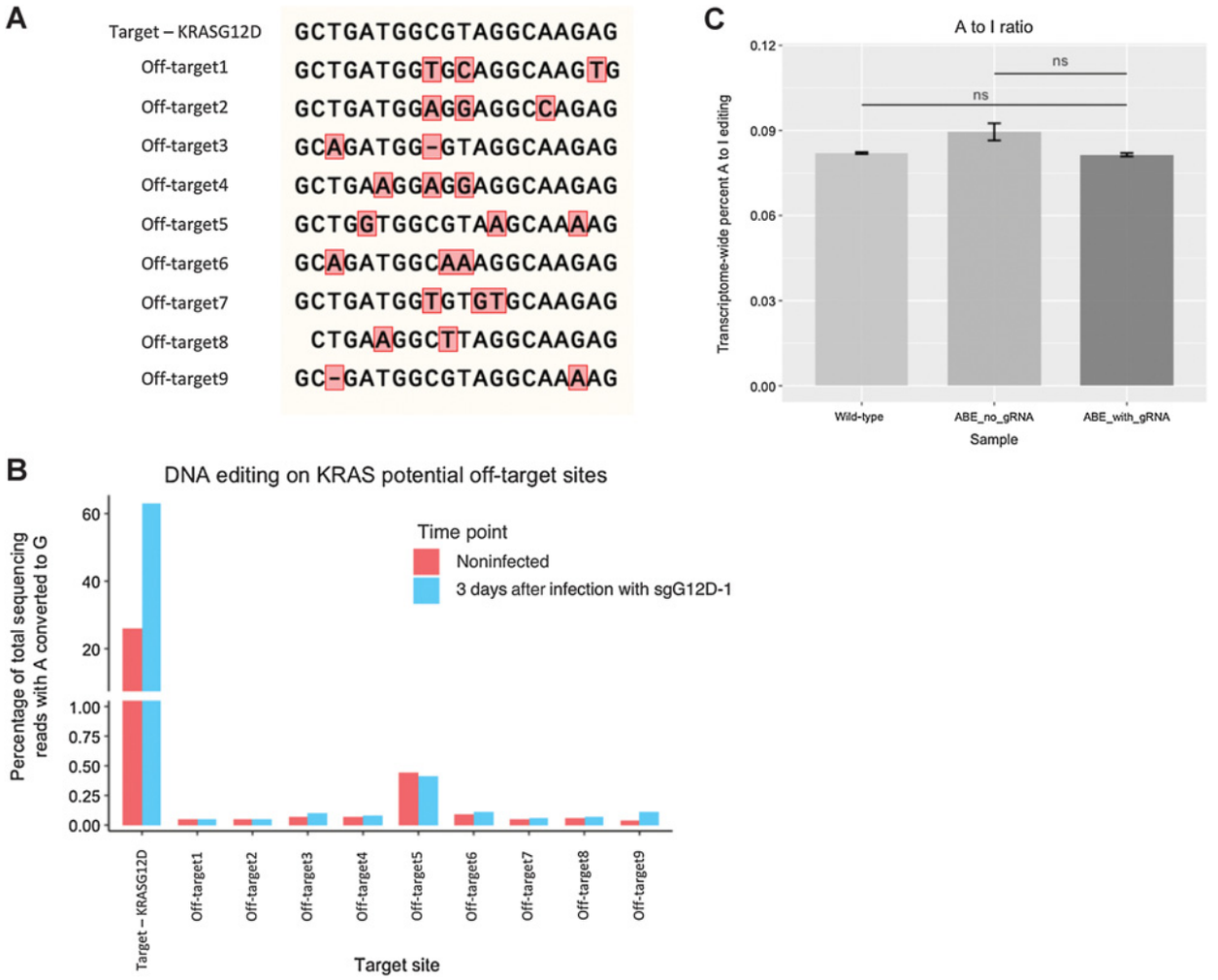

Figure 5.

Off-target analysis for ABE8e in PANC-1 cells. **A,** Alignment of predicted off-target sequences. The on-target sequence is indicated (sgG12D-1) while mismatches to the on-target site are shown in red boxes. **B,** Analysis of deep-sequencing results. The percentages of reads with an "A" to "G" conversion are shown for indicated target sites for control (red) and sgG12D-1–infected cells. **C,** Off-target transcriptome-wide A-to-I conversion analysis in cellular RNA. The error bars represent SEM calculated from two biological replicates.

Finally, we thought to investigate a possible synergy by combining the correction of *KRAS* G12D with *TP53* R273H in PANC-1 cells. Towards this goal, we cloned the *TP53* sgR273H in a BFP-expressing lentiviral vector and co-infected cells with the *KRAS* sgG12D-TdTomato lentivirus. We then followed single- and TdTomato-BFP double positive cells over time. Importantly, RKO cells (*KRAS* WT, *TP53* WT) did not show any growth disadvantage in response to double- or single infections with sgG12D-TdTomato and sgR273H-BFP containing viruses (**Fig. 6E**). In contrast, we observed a sharp decline of the double positive population that was significantly stronger than the decline of the single positive cells (**Fig. 6E**; Supplementary Fig. S7), suggesting that co-repair of mutant *KRAS* and *TP53* has an additive effect in eliminating corrected cells.

Base editing in mutant *KRAS* and *TP53* PDOs

To move cancer-driver base editing closer to translational implementation, we employed a more clinically-relevant culture model and investigated the approach in *KRAS* G12D-mutant PDOs. Base editing was performed in a *KRAS*-G12D mutant PDO (DD442) and a *KRAS* WT PDO control line (DD107) and the effects were analyzed utilizing the established competition assay (**Fig. 7A**). In infected DD107 control organoids, no change in the percentage of TdTomato-positive cells versus noninfected cells was observed with the sgRNA1-G12D, demonstrating that expression of NG-ABE in conjunction with sgG12D-1 is well tolerated in PDOs with a *KRAS* WT background. In contrast, we detected a progressive, albeit slow decline in TdTomato-positive cells over time in the DD442 PDO (**Fig. 7B**). Although the depletion was not as efficient as in the G12D mutant PANC-1 cell line, we detected >30% correctly edited A>G bases 10 days after infection (**Fig.7C**; Supplementary Fig. S8).

To extend the approach to a different tumor type and to a different oncogenic mutation, we targeted a hemizygous *TP53* hotspot mutation (p.R175H, c.524G>A) in the colorectal carcinoma PDO line DD663 (**Fig. 8A**). Remarkably, a rapid decline of TdTomato-positive cells was

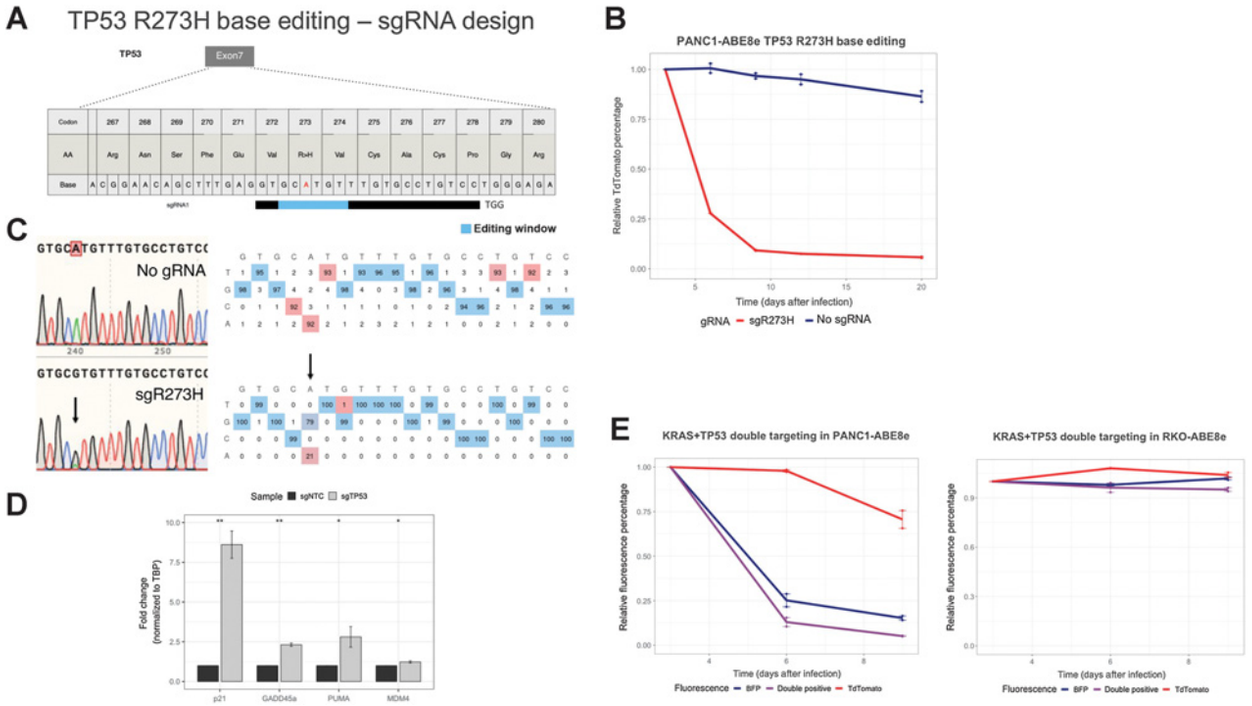

Figure 6.

Base editing of mutant *TP53* R273H in PANC-1 cells. **A,** Overview of the employed sgRNA to repair the R273H mutation. sgRNA alignment with respect to the mutation (red "A") is shown. The hypothetical editing window (blue) and the chosen PAM sequence are presented. **B,** Time course of *TP53* R273H base editing in PANC-1 cells. The relative abundance of cells treated with the sgRNA (sgR273H, red) in addition to an empty vector control (no sgRNA, blue) is shown as the percentage of TdTomato-positive cells over time, relative to 3 days after infection. Error bars represent means ± SD from biological triplicates performed in three independent experiments. **C,** Left, representative chromatograms of cells treated with sgR273H (bottom) in comparison with cells treated with the empty vector control (top) at 3 dpi. The R273H mutation is highlighted in a red box. The edited "A" is indicated by an arrow. EditR quantification of base editing efficiency indicating the 20 bp sgR273H sequence, representing base percentages of the empty vector control (top) and edited base percentages in cells treated with sgR273H (bottom). The edited "A" is indicated by an arrow. **D,** RT-qPCR for p21, PUMA, GADD, MDM4, normalized to TBP as a housekeeping gene on RNA isolated at 48 hours after infection, from PANC-1 cells treated with the sgR273H sgRNA or with a nontargeting control sgRNA. Significance was assessed by a paired Student *t* test comparing the fold change of the assessed genes in the p53 sgRNA sample to that of sgNTC. *, $P < 0.05$; **, $P < 0.01$; $N = 3$. **E,** Time course of double targeting of KRAS G12D and *TP53* R273H base editing in PANC-1 and RKO cells. The relative abundance of cells infected with sgR273H-BFP in conjunction with sgG12D-TdTomato is shown as the relative percentage of fluorescence over time, relative to 3 days after infection. Error bars represent means ± SD from biological replicates performed in two independent experiments.

observed, reaching less than 25% of TdTomato-positive cells 20 days after infection (**Fig. 8B**), suggesting that the infected cells were depleted and largely outcompeted by noninfected cells. Concomitantly, PCR amplification of *TP53* exon four 3 days after infection with the sgR175H-TdTomato lentivirus and subsequent Sanger sequencing revealed >70% of A>G conversions, signifying efficient and rapid correction back to the wild-type *TP53* sequence (**Fig. 8C**). These results demonstrate for the first time that BE-mediated correction of oncogenic mutations is possible in PDOs and that this correction impedes cancer organoid growth.

Discussion

Programmable nucleases enable the targeting of specific genomic sequences including cancer driver mutations. Mutated in one quarter of cancer patients, *KRAS* represents the most frequently mutated oncogene in human cancers (3), whereas its pharmacologic inhibition is limited (4). We demonstrate that different *KRAS* mutations can be selectively targeted using *Streptococcus pyogenes* CRISPR-Cas9 nuclease, even though the difference from the wild-type allele is only a single nucleotide. Cleaving *KRAS* mutant variants in the classical 2D cell lines HCT116, A549, and PANC-1 cells rapidly depleted targeted cells up to 80%, a finding that is in line with previous studies, suggesting that many cancer cells are genetically dependent on *KRAS* mutations (8, 37, 38). However, long-term expression of Cas9 also selected for oncogenic escape variants that were resistant to targeting with the original sgRNA. In recent years, two studies have successfully used CRISPR-based cleavage of *KRAS* mutations G12V, G12D, and G13D and concluded that this approach can potentially be used for the treatment of patients with cancer (39, 40). In contrast to our study, these studies did not report the occurrence of oncogenic escape clones following Cas9 treatment. Considering these results, our work urges caution with Cas9 nuclease-based approaches to disable activating mutations in oncogenes, especially when such an approach is sought for potential clinical applications.

The development of second-generation ABE variants with increased deaminase activity (28) together with broadened compatibility with Cas homologs provided the opportunity for these genome editing tools to be tested for the correction of cancer mutations. Our work pioneers this approach for *KRAS* and *TP53* mutations. Our results demonstrate that *KRAS* mutation correction was possible in all tested cell lines, although with different success rates. In A549 cells

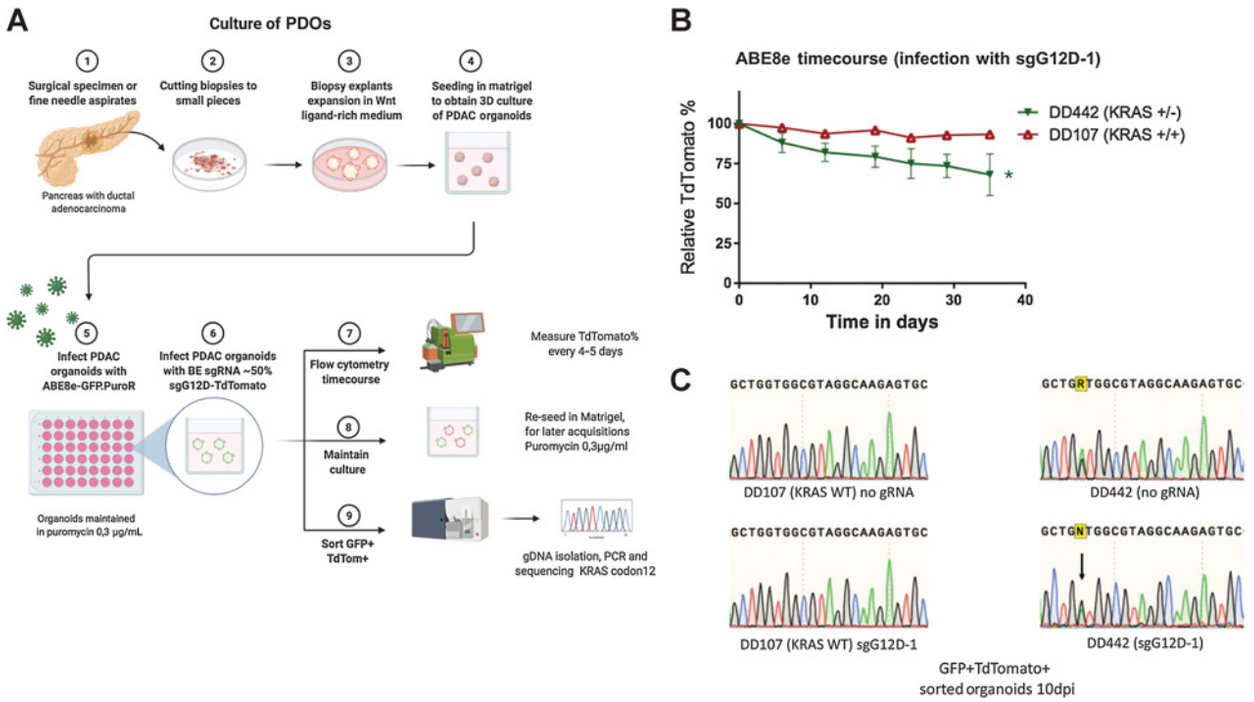

Figure 7.

Base editing of mutant *KRAS* G12D in PDOs. **A,** Graphical presentation of the experimental set-up for base editing in organoids. Important steps are indicated by arrows. **B,** Time course of *KRAS* G12D base editing in indicated organoid lines. The relative abundance of cells treated with the G12D targeting sgRNA (sgG12D-1) in both lines is shown as the percentage of TdTomato-positive cells over time, relative to 5 days after infection, the initial time point for measuring TdTomato signal. Error bars represent means ± SD from biological triplicates performed in three independent experiments. Significance was assessed by Student *t* test comparing the mean percentage at end points of experimental sgRNA to that of no sgRNA. *, $P < 0.05$. **C,** Representative chromatograms of *KRAS* codon 12 treated with an empty vector control (top) and with sgG12D-1 (bottom) for the indicated organoid lines, at 10 days after infection. The edited "A" in the DD442 line is highlighted by an arrow.

bearing the G12S variant, all four sgRNAs showed progressive depletion and editing. A weak bystander editing was also observed at a neighboring adenine, yielding a silent mutation. In contrast, in HCT116 cells, only one sgRNA showed a measurable depletion, despite similar sequences of the sgRNAs. This could be owing to the position of codon 13 and the targeted "A" within the editing window, as well as the unpredictable sequence preference of the deaminase. This result encourages for the testing of several sgRNAs per mutation, harnessing different PAMs, sgRNA lengths, and target "A" position within the editing window. A machine learning model (BE-Hive) has been recently described to predict editing efficiencies of several base editors across different target sites (41). It would be interesting to evaluate, if this algorithm can predict the efficiency and specificity of sgRNAs to correct cancer mutations in cells. Other strategies to improve editing efficiencies include the use of alternative Cas9 homologs compatible with ABE8e, which are available with different PAM preferences (28), or using an ABE where TadA replaces the Cas9 HNH-domain, allowing for an alternative editing window (42). Furthermore, base editors with optimized architectures, such as rigid linkers have recently been described (43), which might improve base editing of cancer mutations. Nevertheless, potentially harmful bystander edits always have to be considered, as we observed for the *KRAS* G13D correction, where editing of a bystander "A" in a subset of cells caused an amino acid change, possibly leading to an oncogenic variant. Importantly, these bystander edits can be predicted and their consequences can be evaluated beforehand. Nevertheless, versions of base editors that reduce bystander edits would further improve their utility (44).

Remarkably, in PANC-1 cells bearing the G12D variant, base edited cells showed substantial levels of editing and were depleted almost entirely, after treatment with two independent sgRNAs. Moreover, base editing depletion dynamics seemed comparable with the nuclease approach (compare **Figs. 1B** and **4B**). However, base editing seems to be advantageous, because in contrast to the nuclease approach, we managed to deplete the ABE expressing cells almost entirely, without the occurrence of escape variants. Although this result illustrates the robustness and accuracy of the base editing approach to correct the oncogenic driver mutations, it also highlights that some rare cells still escape the consequence of oncogene mutation correction, likely representing a reservoir of resistant clones that would ultimately result in clinical relapse. It will be interesting to molecularly study these resistant cells in the future, as they could reveal mechanisms how cancer cells can bypass their *KRAS* dependency.

The time-lapse microscopy experiments revealed the phenotypic consequences of *KRAS* correction in PANC-1 cells. Although sequencing revealed that the correction within the cells happens rather quickly (>50% at 3dpi; Supplementary Fig. S5A), cells carrying the sgG12D-1 did not all die or arrest at this early time point. Instead, several dividing red cells seemed healthy during the observation period, suggesting that these cells survive the *KRAS* correction for an extended period of time. It is known that constitutive *KRAS* activation boosts several key aspects of cancer cell metabolism such as glycolysis, micropinocytosis, and autophagy to maintain high-energy levels (45, 46). Hence, cells with higher metabolites might persist longer after the correction of the *KRAS* mutation (47). Moreover, recent characterization of PANC-1

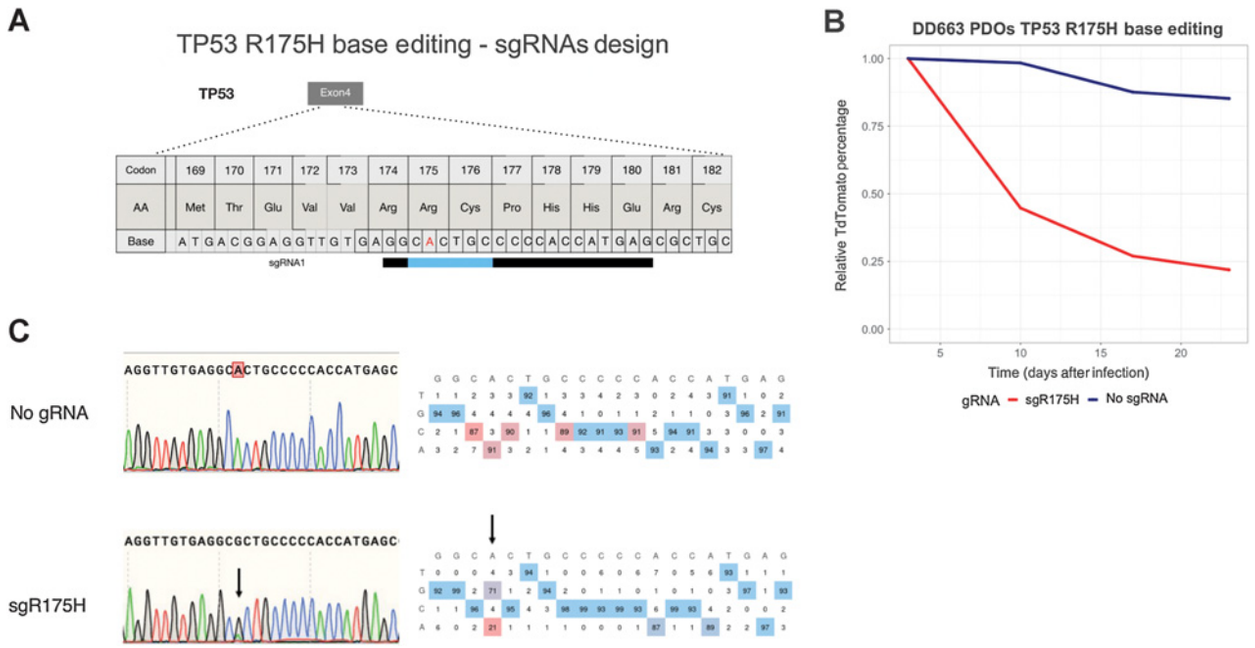

Figure 8.

Base editing of mutant TP53 R175H in PDOs. **A,** Overview of the employed sgRNA to repair the R175H mutation (sgR175H). An sgRNA alignment with respect to the mutation (red "A") is shown. **B,** Time course of TP53 R175H base editing in DD663 organoids. The relative abundance of cells treated with the R175H targeting sgRNA (sgR175H) in addition to an empty vector control is shown as the percentage of TdTomato-positive cells over time, relative to 3 days after infection, the initial time point for measuring TdTomato signal ($N = 1$). **C,** Representative chromatograms of cells treated with sgR175H (bottom) in comparison with cells treated with the empty vector control (top) at 3 days post infection. The R175H mutation is highlighted in a red box. The edited "A" is indicated by an arrow. EditR quantification of base editing efficiency indicating the 20 bp sequence of sgR175H, representing base percentages of the empty vector control (top) and edited base percentages in cells treated with sgR175H (bottom). The edited "A" is indicated by an arrow.

cells has revealed a pleomorphic phenotype with differential stem cell marker expression (48). It is therefore possible that the heterogenicity within the cells in culture accounts for the divergent behavior observed.

We extended the base editing approach to correct cancer mutations in tumor suppressors, namely the tumor suppressor *TP53*. Of note, many *TP53* missense mutations are G>A missense mutations and are therefore addressable, in particular with Cas9 variants with modified PAM preferences. Intriguingly, the recovery of only one wildtype allele of the hemizygous *TP53* mutation was sufficient to reactivate p53 function that led to a sharp depletion of corrected cells, likely triggered through p53-mediated upregulation of cell-cycle/apoptosis regulator genes, such as *p21*, *GADD45A*, *MDM4*, and *PUMA*. Of particular relevance, *TP53* is the most common *KRAS* co-mutation at 39.4% (49), a fact that has profound implications for prognosis (50). The demonstration that co-correction of two mutations was possible and led to accelerated depletion of targeted cells offers new perspectives to identify synergistic dependencies in cancer cells. In this context, it will be interesting to investigate whether co-correction of *TP53* and *KRAS* can prevent the emergence of resistant cells, as was observed when *KRAS* G12D was corrected alone.

Moving closer to the clinic, PDOs were tested in terms of their accessibility for base editing. An edited PDO with a *KRAS*G12D mutation demonstrated a progressive depletion, albeit less efficient than in the PANC-1 cells, employing the same sgG12D-1. Importantly though, the *KRAS* wild-type PDO showed no signs of sensitivity towards the ABE8e-sgG12D-1 complex even after 1 month of treatment. Moreover, sequencing of sorted *KRAS* wild-type PDO demonstrated only *KRAS* WT at codon 12, without signs of any editing of "A" bases. In contrast, sequencing of treated G12D mutant PDO carrying the ABE8e-sgG12D-1 complex revealed an editing efficiency of >30%, indicating that slow regression of infected cells seems to reflect a slower editing kinetics. Why the base editing appears to be slower in pancreatic organoids is not apparent at first glance, but strategies to enhance base editing efficiency in PDOs seem feasible. For example, lower base editing efficiency in organoids could be due to the presence of agents in the organoid media influencing the base editing reaction. Fibroblast growth factor (FGF) 10 in the organoid medium may mask *KRAS* dependence by facilitating activation of the MAPK pathway via the PI3K–AKT axis (51). In addition, possible patient-specific mutational and transcriptional signatures (e.g., DNA repair fidelity) might influence the efficiency of the base editing reaction. Adaptation of the organoid culture conditions might allow more efficient base editing by testing base editing in growth factor reduced culture conditions. Although different mutations/sgRNAs were exploited, more efficient base editing was observed in the colorectal cancer PDO for a *TP53* hotspot mutation, indicating that tissue origin of the cancer cells might also influence base editing efficiencies. However, already without further possible improvements, our study demonstrates that base editing technology can be harnessed to correct driver mutations in cancer organoids. This finding allows for testing the vulnerability of individual tumors *in vitro* to phenotypically profile these cells.

To our knowledge, this is the first study demonstrating efficient targeting of oncogenic recurrent mutations in activated oncogenes and tumor suppressor genes using base editing in both classical 2D cell lines and organoids. Undeniably, the development of base editors for cancer

therapy is challenging because in order to be very efficient, every cancer cell in the body would have to be reached. However, only in the past two years, base editors have progressed towards clinical use for several diseases, providing proof-of-concept for the use of base editing *in vivo* (52). As base editors continue to advance towards clinical applications, their continued optimization to maximize their efficacy, specificity, and ability to target cancer cells *in vivo* remain important priorities (53, 54). Given the rapid development of base editing technology (55, 56) and delivery (57), we speculate that correction of cancer driver mutations by base editing may become a therapeutic modality in the future.

Authors' Disclosures

F. Buchholz reports grants from DKFZ/DKTK and EU during the conduct of the study. No disclosures were reported by the other authors.

Authors' Contributions

S. Sayed: Conceptualization, validation, investigation, visualization, writing–original draft, writing–review and editing. **O.A. Sidorova:** Investigation, visualization, writing–review and editing. **A. Hennig:** Investigation. **M. Augsburg:** Methodology. **C.P. Cortés Vesga:** Investigation. **M. Abohawya:** Formal analysis, visualization. **L.T. Schmitt:** Validation. **D. Sürün:** Validation, writing–review and editing. **D.E. Stange:** Resources, writing–review and editing. **J. Mircetic:** Investigation, writing–review and editing. **F. Buchholz:** Conceptualization, resources, supervision, funding acquisition, writing–review and editing.

Acknowledgments

The project was financially supported by the European commission H2020 UPGRADE, grant no. 825825 (to S. Sayed) and Deutsches Krebsforschungszentrum (DKFZ Heidelderg): DKTK Joint Funding Program "Breaking therapy resistance in AML (RiskY-AML)." The authors would like to thank all members of the Buchholz lab for the fruitful discussions. Graphical schemes were created with www.BioRender.com.

The costs of publication of this article were defrayed in part by the payment of page charges. This article must therefore be hereby marked *advertisement* in accordance with 18 U.S.C. Section 1734 solely to indicate this fact.

Note

Supplementary data for this article are available at Cancer Research Online (http://cancerres.aacrjournals.org/).

Received August 2, 2021; revised August 19, 2021; accepted June 29, 2022; published first July 8, 2022.

References

1. Prior IA, Hood FE, Hartley JL. The frequency of Ras mutations in cancer. Cancer Res 2020;80:2969–74.
2. Cox AD, Fesik SW, Kimmelman AC, Luo J, Der CJ. Drugging the undruggable RAS: mission possible? Nat Rev Drug Discov 2014;13:828–51.
3. Haigis KM. KRAS alleles: the devil is in the detail. Trends Cancer 2017;3:886–97.
4. Papke B, Der CJ. Drugging RAS: know the enemy. Science 2017;355:1158–63.
5. Ostrem JML, Shokat KM. Direct small-molecule inhibitors of KRAS: from structural insights to mechanism-based design. Nat Rev Drug Discov 2016;15:771–85.
6. Christensen JG, Olson P, Briere T, Wiel C, Bergo MO. Targeting Kras g12c-mutant cancer with a mutation-specific inhibitor. J Intern Med 2020;288:183–91.
7. Skoulidis F, Li BT, Dy GK, Price TJ, Falchook GS, Wolf J, et al. Sotorasib for lung cancers with KRAS p.G12C mutation. N Engl J Med 2021;384:2371–81.
8. Tsherniak A, Vazquez F, Montgomery PG, Weir BA, Kryukov G, Cowley GS, et al. Defining a cancer dependency map. Cell 2017;170:564–70.
9. Yuan TL, Fellmann C, Lee CS, Ritchie CD, Thapar V, Lee LC, et al. Development of siRNA payloads to target KRAS-mutant cancer. Cancer Discov 2014;4:1182–97.
10. Bäumer S, Bäumer N, Appel N, Terheyden L, Fremerey J, Schelhaas S, et al. Antibody-mediated delivery of anti-KRAS-siRNA in vivo overcomes therapy resistance in colon cancer. Clin Cancer Res 2015;21:1383–94.
11. Gebler C, Lohoff T, Paszkowski-Rogacz M, Mircetic J, Chakraborty D, Camgoz A, et al. Inactivation of cancer mutations utilizing CRISPR/Cas9. J Natl Cancer Inst 2017;109:1546.
12. Li X, Qian X, B Wang, Xia Y, Zheng Y, Du L, et al. Programmable base editing of mutated TERT promoter inhibits brain tumour growth. Nat Cell Biol 2020;22:282–8.
13. Heckl D, Kowalczyk MS, Yudovich D, Belizaire R, Puram RV, McConkey ME, et al. Generation of mouse models of myeloid malignancy with combinatorial genetic lesions using CRISPR-Cas9 genome editing. Nat Biotechnol 2014;32:941–6.
14. Chen B, Gilbert LA, Cimini BA, Schnitzbauer J, Zhang W, Li G-W, et al. Dynamic imaging of genomic Loci in living human cells by an optimized CRISPR/Cas system. Cell 2013;155:1479–91.
15. Ran FA, Hsu PD, Wright J, Agarwala V, Scott DA, Zhang F. Genome engineering using the CRISPR-Cas9 system. Nat Protoc 2013;8:2281–308.
16. Zafra MP, Schatoff EM, Katti A, Foronda M, Breinig M, Schweitzer AY, et al. Optimized base editors enable efficient editing in cells, organoids and mice. Nat Biotechnol 2018;36:888–93.
17. Sayed S, Paszkowski-Rogacz M, Schmitt LT, Buchholz F. CRISPR/Cas9 as a tool to dissect cancer mutations. Methods 2019;164–165:36–48.
18. Hennig A, Wolf L, Jahnke B, Polster H, Seidlitz T, Werner K, et al. CFTR Expression analysis for subtyping of human pancreatic cancer organoids. Stem Cells Int 2019;2019:1–8.
19. Seidlitz T, Merker SR, Rothe A, Zakrzewski F, Neubeck von C, Grützmann K, et al. Human gastric cancer modelling using organoids. Gut 2019;68:207–17.
20. Kluesner MG, Nedveck DA, Lahr WS, Garbe JR, Abrahante JE, Webber BR, et al. EditR: a method to quantify base editing from sanger sequencing. CRISPR J 2018;1:239–50.
21. Clement K, Rees H, Canver MC, Gehrke JM, Farouni R, Hsu JY, et al. CRISPResso2 provides accurate and rapid genome editing sequence analysis. Nat Biotechnol 2019;37:224–6.
22. Li H. Minimap2: pairwise alignment for nucleotide sequences. Bioinformatics 2018;34:3094–100.
23. Lawrence M, Huber W, Pagès H, Aboyoun P, Carlson M, Gentleman R, et al. Software for computing and annotating genomic ranges. PLoS Comput Biol 2013;9:e1003118EP.
24. Dobin A, Davis CA, Schlesinger F, Drenkow J, Zaleski C, Jha S, et al. STAR: ultrafast universal RNA-seq aligner. Bioinformatics 2013;29:15–21.
25. Picardi E, Pesole G. REDItools: high-throughput RNA editing detection made easy. Bioinformatics 2013;29:1813–4.
26. Rees HA, Liu DR. Base editing: precision chemistry on the genome and transcriptome of living cells. Nat Rev Genet 2018;19:770–88.
27. Nishimasu H, Shi X, Ishiguro S, Gao L, Hirano S, Okazaki S, et al. Engineered CRISPR-Cas9 nuclease with expanded targeting space. Science 2018;361:1259–62.
28. Richter MF, Zhao KT, Eton E, Lapinaite A, Newby GA, Thuronyi BW, et al. Phage-assisted evolution of an adenine base editor with improved Cas domain compatibility and activity. Nat Biotechnol 2020;38:883–91.
29. Pruitt K, Pestell RG, Der CJ. Ras inactivation of the retinoblastoma pathway by distinct mechanisms in NIH 3T3 fibroblast and RIE-1 epithelial cells. J Biol Chem 2000;275:40916–24.
30. Agbunag C, Bar-Sagi D. Oncogenic K-ras drives cell cycle progression and phenotypic conversion of primary pancreatic duct epithelial cells. Cancer Res 2004;64:5659–63.
31. Fan J, Bertino JR. K-ras modulates the cell cycle via both positive and negative regulatory pathways. Oncogene 1997;4:2595–607.
32. Bae S, Park J, Kim J-S. Cas-OFFinder: a fast and versatile algorithm that searches for potential off-target sites of Cas9 RNA-guided endonucleases. Bioinformatics 2014;30:1473–5.
33. Xin H, Wan T, Ping Y. Off-Targeting of Base Editors: BE3 but not ABE induces substantial off-target single nucleotide variants. Signal Transduct Target Ther 2019;4:9.

34. Grünewald J, Zhou R, Garcia SP, Iyer S, Lareau CA, Aryee MJ, et al. Transcriptome-wide off-target RNA editing induced by CRISPR-guided DNA base editors. Nature 2019;569:433–7.
35. Kastenhuber ER, Lowe SW. Putting p53 in context. Cell 2017;170:1062–78.
36. Hu J, Cao J, Topatana W, Juengpanich S, Li S, Zhang B, et al. Targeting mutant p53 for cancer therapy: direct and indirect strategies. J Hematol Oncol 2021;14:157.
37. Steckel M, Molina-Arcas M, Weigelt B, Marani M, Warne PH, Kuznetsov H, et al. Determination of synthetic lethal interactions in KRAS oncogene-dependent cancer cells reveals novel therapeutic targeting strategies. Cell Res 2012;22:1227–45.
38. Dwane L, Behan FM, Gonçalves E, Lightfoot H, Yang W, van der Meer D, et al. Project score database: a resource for investigating cancer cell dependencies and prioritizing therapeutic targets. Nucleic Acids Res 2020;6:38–8.
39. Lee W, Lee JH, Jun S, Lee JH, Bang D. Selective targeting of KRAS oncogenic alleles by CRISPR/Cas9 inhibits proliferation of cancer cells. Sci Rep 2018; 811879.
40. Kim W, Lee S, Kim HS, Song M, Cha YH, Kim Y-H, et al. Targeting mutant KRASwith CRISPR-Cas9 controls tumor growth. Genome Res 2018;28:374–82.
41. Arbab M, Shen MW, Mok B, Wilson C, Matuszek Ż, Cassa CA, et al. Determinants of base editing outcomes from target library analysis and machine learning. Cell 2020;182:643–80.
42. Chu SH, Packer M, Rees H, Lam D, Yu Y, Marshall J, et al. Rationally designed base editors for precise editing of the sickle cell disease mutation. CRISPR J 2021; 4:169–77.
43. Tan J, Zhang F, Karcher D, Bock R. Engineering of high-precision base editors for site-specific single nucleotide replacement. Nat Commun 2019;10:439.
44. Grünewald J, Zhou R, Iyer S, Lareau CA, Garcia SP, Aryee MJ, et al. CRISPR DNA base editors with reduced RNA off-target and self-editing activities. Nat Biotechnol 2019;37:1041–48.
45. Kerk SA, Papagiannakopoulos T, Shah YM, Lyssiotis CA. Metabolic networks in mutant KRAS-driven tumours: tissue specificities and the microenvironment. Nat Rev Cancer 2021;21:510–25.
46. Pupo E, Avanzato D, Middonti E, Bussolino F, Lanzetti L. KRAS-Driven metabolic rewiring reveals novel actionable targets in cancer. Front Oncol 2019;9:848.
47. Kamphorst JJ, Nofal M, Commisso C, Hackett SR, Lu W, Grabocka E, et al. Human pancreatic cancer tumors are nutrient poor and tumor cells actively scavenge extracellular protein. Cancer Res 2015;75:544.
48. Gradiz R, Silva HC, Carvalho L, Botelho MF, Mota-Pinto A. MIA PaCa-2 and PANC-1 – pancreas ductal adenocarcinoma cell lines with neuroendocrine differentiation and somatostatin receptors. Sci Rep 2016;6:21648.
49. Scheffler M, Ihle MA, Hein R, Merkelbach-Bruse S, Scheel AH, Siemanowski J, et al. K-ras mutation subtypes in NSCLC and associated co-occuring mutations in other oncogenic pathways. JTO Acquisition 2019;14:606–16.
50. Salgia R, Pharaon R, Mambetsariev I, Nam A, Sattler M. The improbable targeted therapy: KRAS as an emerging target in non-small cell lung cancer (NSCLC). Cell Rep Med 2021;2:100186.
51. Ndlovu R, Deng LC, Wu J, Li XK, Zhang JS. Fibroblast growth factor 10 in pancreas development and pancreatic cancer. Front Genet 2018;9:482.
52. Levy JM, Yeh W-H, Pendse N, Davis JR, Hennessey E, Butcher R, et al. Cytosine and adenine base editing of the brain, liver, retina, heart and skeletal muscle of mice via adeno-associated viruses. Nat Biomed Eng 2020;4:97–110.
53. Zeng J, Wu Y, Ren C, Bonanno J, Shen AH, Shea D, et al. Therapeutic base editing of human hematopoietic stem cells. Nat Med 2020;26:535–41.
54. Musunuru K, Chadwick AC, Mizoguchi T, Garcia SP, DeNizio JE, Reiss CW, et al. In vivo CRISPR base editing of PCSK9 durably lowers cholesterol in primates. Nature 2021;593:429–34.
55. Lim K, Cho S-I, Kim J-S. Nuclear and mitochondrial DNA editing in human cells with zinc finger deaminases. Nat Commun 2022;13:366.
56. Xu X, Chemparathy A, Zeng L, Kempton HR, Shang S, Nakamura M, et al. Engineered miniature CRISPR-Cas system for mammalian genome regulation and editing. Mol Cell 2021;81:4333–4.
57. Banskota S, Raguram A, Suh S, Du SW, Davis JR, Choi EH, et al. Engineered virus-like particles for efficient *in vivo* delivery of therapeutic proteins. Cell 2022; 185:250–65.